Current Biology, Vol. 15, 684–689, April 12, 2005, ©2005 Elsevier Ltd All rights reserved. DOI 10.1016/j.cub.2005.02.061

Direct Observation Demonstrates that Liprin-α Is Required for Trafficking of Synaptic Vesicles

Kyle E. Miller,[1] Jamin DeProto,[1] Nancy Kaufmann,[1,2] Bharatkumar N. Patel,[1] April Duckworth,[1] and David Van Vactor[1,*]
[1]Department of Cell Biology and Program in Neuroscience
Harvard Medical School
Boston, Massachusetts 02115

Summary

Axonal transport is required for the elaboration and maintenance of synaptic morphology and function [1, 2]. Liprin-αs are scaffolding proteins [3] important for synapse structure and electrophysiology [4]. A reported interaction with Kinesin-3 (Kif1a) suggested Liprin-α may also be involved in axonal transport [5]. Here, at the light and ultrastructural levels, we discover aberrant accumulations of synaptic vesicle markers (Synaptotagmin and Synaptobrevin-GFP) and clear-core vesicles along *Drosophila Liprin-α* mutant axons. Analysis of presynaptic markers reveals reduced levels at *Liprin-α* synapses. Direct visualization of Synaptobrevin-GFP transport in living animals demonstrates a decrease in anterograde processivity in *Liprin-α* mutants but also an increase in retrograde transport initiation. Pull-down assays reveal that Liprin-α interacts with *Drosophila* Kinesin-1 (Khc) but not dynein. Together, these findings suggest that Liprin-α promotes the delivery of synaptic material by a direct increase in kinesin processivity and an indirect suppression of dynein activation. This work is the first to use live observation in *Drosophila* mutants to demonstrate the role of a scaffolding protein in the regulation of bidirectional transport. It suggests the synaptic strength and morphology defects linked to *Liprin-α* [4, 6] may in part be due to a failure in the delivery of synaptic-vesicle precursors [7].

Results and Discussion

Liprin-αs are well-conserved proteins initially identified through their association with the receptor protein tyrosine phosphatase LAR [8]. In vertebrates, *C. elegans*, and *Drosophila*, functional studies demonstrated that Liprin-α is a determinant of synapse structure and electrophysiology [4, 9, 10]. Biochemical studies suggested that Liprin-α acts as a scaffolding protein for several synaptic proteins [11]. However, the finding that mammalian Liprin-α associates with a Kinesin-3 family member, Kif1A [5], raised the question of whether during neuronal differentiation Liprin-α is directly involved in axonal transport of synaptic components [7].

Disruption of *Liprin-α* leads to defects in synaptic morphology and function similar to those observed in kinesin mutants [1, 4, 9, 12]. A phenotypic hallmark of defective axon transport is the accumulation of synaptic vesicles along the axon [2]. Therefore, we examined the distribution of synaptotagmin (Syt), which is a component of synaptic vesicle precursors (SVPs) [13]. In wild-type *Drosophila* third-instar larva, wide-field fluorescence microscopy revealed faint and evenly distributed Syt staining along the peripheral nerves [Figure 1A′]. However in *Liprin-α* mutants, abnormal punctate Syt accumulations occurred along the axonal length [Figure 1B′]. Similar accumulations were observed with the independent marker green-fluorescent-protein (GFP)-tagged synaptobrevin (nSyb-GFP [14]) under the motor neuron GAL4 driver D42 [Figures 1C–1E]. These fully penetrant axonal phenotypes were similar to those found in mutants lacking the *Drosophila* Kinesin-1 family member (*Khc*) [2].

Quantification of SVP marker distribution (see the Supplemental Experimental Procedures available with this article online) demonstrated a 10-fold increase of endogenous Syt in *Liprin-α* mutant axons compared to wild-type controls [Figure 1F] and a 4-fold increase in the number nSyb-GFP puncta in *Liprin-α* mutant motor axons in the peripheral nerves as compared to controls [Figure 1G]. In contrast, we did not see abnormal distributions of mitochondria or the microtubule-associated protein Futsch/MAP1b in *Liprin-α* mutants (data not shown). These findings suggested that Liprin-α is necessary for efficient transport of SVPs.

Although axonal accumulation of Syt and nSyb-GFP suggested transport disruption, alternative explanations included the formation of ectopic synapses, failure in axon integrity, and disruptions of microtubules. To investigate, we used serial-section electron microscopy (EM). Comparing wild-type and *Liprin-α* mutant peripheral nerves revealed accumulations of clear-core vesicles in mutant axons [Figures 2A–2C], reminiscent of *Drosophila* Kinesin-1 family *Khc* mutants [2]. These vesicles resemble those associated with nSyb and Synaptophysin in previous studies [7]. Quantification of vesicle density showed that vesicles accumulate to high numbers in mutant axons and that accumulations are four times more likely to occur than in the wild-type [Figures 2D, 2E, and 2F]. However, we found no ectopic presynaptic specializations, breakdowns in the plasma membrane, or obvious changes in microtubule density or morphology [Figures 2A–2C]. These data support a model in which Liprin-α is required for efficient axonal membrane traffic.

To determine if disruption of *Liprin-α* decreases the delivery of synaptic markers to the neuromuscular junction (NMJ), we examined the levels of nSyb-GFP and the active-zone marker NC82 by using the neuronal marker HRP as an internal control [15]. We found nSyb-GFP (n = 46 NMJs from 12 control animals and 41 NMJs from 11 *Liprin-α* mutants) and NC82 (n = 32 NMJs from eight animals for controls and 24 NMJs from six animals for *Liprin-α* mutants) were significantly reduced by

*Correspondence: davie@hms.harvard.edu
[2]Present address: Department of Biological Science, University of Pittsburgh, Pittsburgh, Pennsylvania 15250.

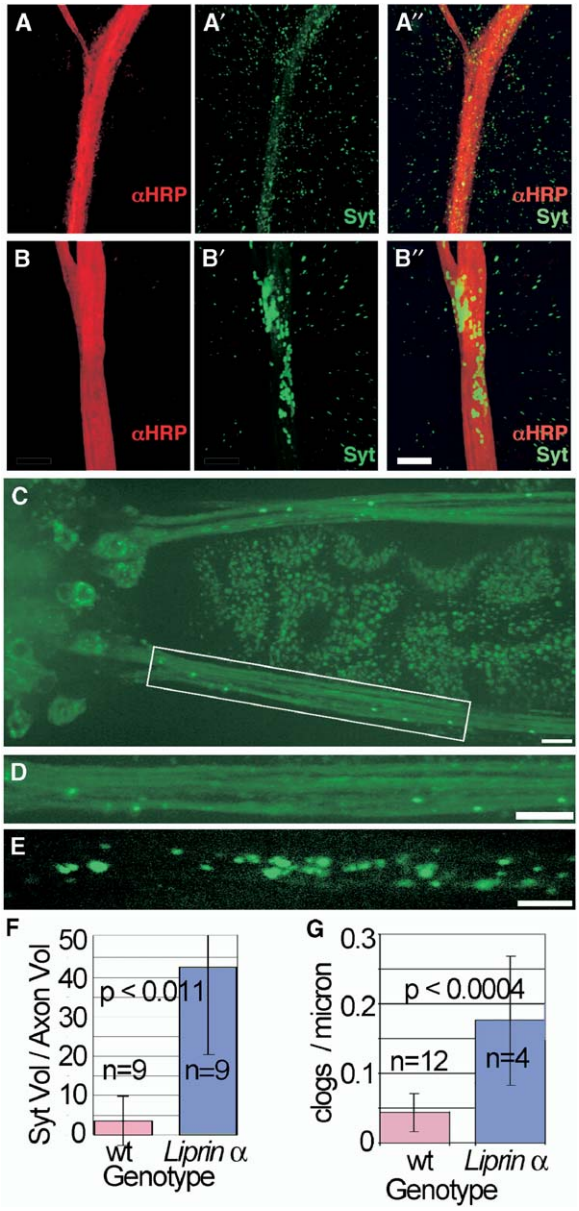

Figure 1. Loss of *Liprin-α* Leads to Accumulations of Synaptic Markers in the Axon

(A) A wild-type nerve stained with HRP and Syt is compared to (B) a *Liprin-α* mutant axon. The scale bar represents approximately 8 μm. (C) nSyb-GFP distribution in motor neurons of control larvae; the scale bar represents 10 μm. (D) Enlargement of inset from panel (C). (E) nSyb-GFP distribution in motor neurons in *Liprin-α* mutants. (F) Quantification of Syt distribution as a fraction of the total axon volume is shown. Error bars show the standard deviation. (G) Quantification of the number of nSyb-GFP accumulations; error bars show the standard deviation (see Supplemental Experimental Procedures).

20% to 29% both in mean levels and in maximum intensity in *Liprin-α* motor terminals compared to controls [Figure 3]. The comparable decrease in both the overall intensity and the peak maximum intensity indicates that the decrease in these protein levels is not simply due to smaller synaptic boutons [4] but to a lower density of synaptic proteins. The failure of *Liprin-α* NMJs to accumulate normal levels of nSyb-GFP and NC82 could result from inefficient active-zone assembly or a disruption in the anterograde transport of these materials.

To directly test whether Liprin-α is required for normal transport of SVPs, we visualized the transport of nSyb-GFP cargo along motor axons in intact third-instar larva by using rapid-scan confocal microscopy [Figures 4A–4H; see Supplemental Experimental Procedures and Movie S1]. To determine the flux of transport, we measured cargo translocation in heterozygous controls and *Liprin-α* homozygous larvae for a total time of 88 min and counted the movement of a total of 1640 nSyb-GFP-positive puncta. For the data in panels 4I, 4J, and 4K, n = 8 animals for the controls and n = 13 animals for the *Liprin-α* homozygous conditions. The results of this analysis reveal that loss of *Liprin-α* significantly decreases the flux of SVPs in the anterograde direction, increases the flux in the retrograde direction, but does not change the total flux [Figure 4I].

Previous studies have suggested coordination between anterograde and retrograde transport [16, 17]. To understand how disruption of *Liprin-α* alters the balance of transport, we measured the number of transition events (stops, starts, and directional reversals for anterograde and for retrograde cargos; in total, 602 events were counted) [Figure 4J]. For each group, the relative probability of an event occurring was normalized based on the levels observed in the control genotype. We found that loss of *Liprin-α* increased the probability that a vesicle moving in the anterograde direction would stop (A to S) by nearly 3-fold but had no effect on the persistence of retrograde transport (R to S) [Figure 4J]. In addition, we found that when vesicles were moving in the anterograde direction or were paused, they were significantly more likely to begin moving in the retrograde direction (anterograde to retrograde and stopped to retrograde) in *Liprin-α* mutants (3.5-fold and nearly 2-fold, respectively) [Figure 4J]. This demonstrates that loss of *Liprin-α* disrupts anterograde traffic by decreasing the processivity of transport and augments retrograde transport by increasing the initiation of retrograde movement.

Synaptic-vesicle precursors are transported by multiple kinesin family members that move with characteristic velocities [7, 18, 19]. To test if decreases in anterograde processivity were due to disruption of a specific kinesin, we measured the velocity of transport and length of time in motion of approximately 6000 vesicles. This analysis did not reveal any consistent alterations in transport velocity profiles between the control and *Liprin-α* groups [Figure 4K]. Instead, the effects on flux [Figure 4I] appear to be due to broad changes that occur in the levels of transport as a result of decreases in kinesin processivity and increases in the initiation of retrograde transport [Figure 4J]. Although this does not rule out a preferential effect on the transport of a subclass of kinesins, it suggests that Liprin-α may regulate multiple types of anterograde motors.

Because Liprin-α promotes anterograde movement and antagonizes retrograde movement, we wondered if it might be part of a motor docking scaffold common to kinesins and dynein. To test this, we used Liprin fusion-protein pull-down assays and examined interactions

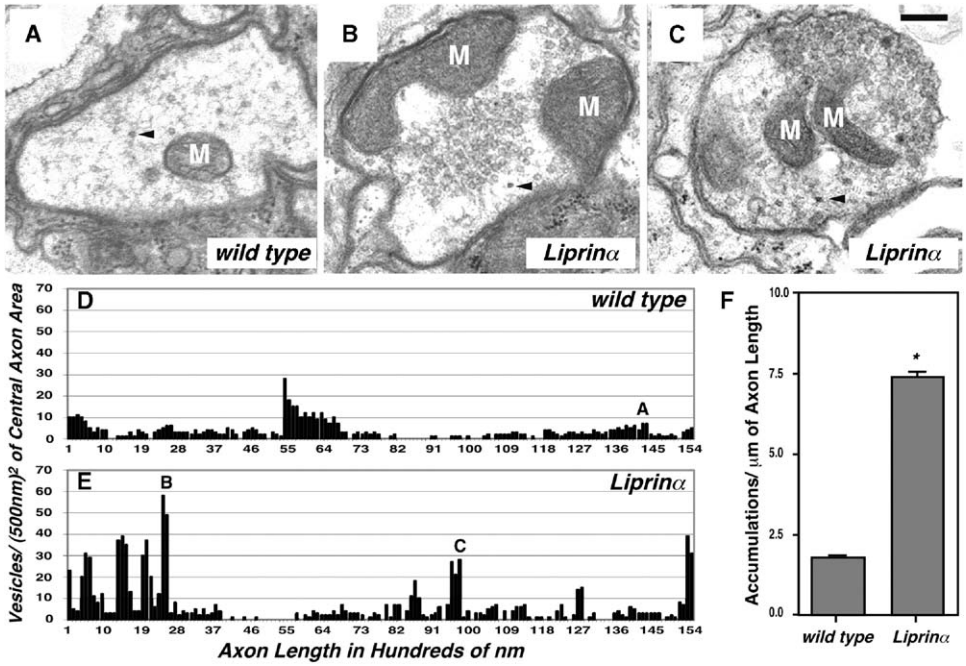

Figure 2. Vesicles Accumulate in *Liprin-α* Mutant Axons

(A) Serial ultrathin sections were examined for anomalous membrane structures, microtubule content, and vesicle clusters. Wild-type axon cross-sections contain microtubules (arrowhead) and a small number of widely distributed clear-core vesicles or other intracellular membrane structures.

(B and C) *Liprin-α* axons contain microtubules (arrowheads), and frequent large aggregations of clear-core vesicles. Mitochondria are denoted by M. The scale bar represents 120 nm.

(D) Vesicle density in wild-type axons has slight variations comparable with light-level observations.

(E) The density of vesicles in a *Liprin-α* mutant axon display frequent peaks.

(F) Each section was also inspected for the presence of more than four contiguous vesicles (see Supplemental Experimental Procedures); this criterion provides a conservative measure of vesicle aggregation. *Liprin-α* axons (n = 187) had an accumulation frequency that was nearly four times that of wild-type axons (n = 144; $\chi^2 = 2.2 \times 10^{-10}$). The standard error of the mean is indicated for each bar in (F).

with dynein and the *Drosophila* Kinesin-1 Khc (see Supplemental Experimental Procedures). We failed to detect an interaction between Liprin-α and dynein [Figure 4L] but found a robust and reproducible association between Kinesin-1 and Liprin-α [Figure 4L]. For controls, GST alone and another member of the Liprin family showed no interactions with Kinesin-1 in this assay [Figure 4L]. The association between Kinesin-1 and Liprin-α raises the question of the site of interaction. Possibilities for direct interaction include a Kinesin-1 region homologous to the Liprin-α binding site on Kif1a [3, 5], as well as the myosin V binding domain on Kinesin-1 [20] because there is homology between Liprin-αs and myosins [21]. Of course, the interaction may also be mediated indirectly through additional components such as kinesin light chain and/or novel sites on Kinesin-1. The ability of Liprin-α to associate with Kinesin-1 suggests that Liprin-α's role in anterograde transport is direct.

Three prominent models have been proposed to explain the regulation of bidirectional transport: (1) a substitution model in which only one set of motors is present on the cargo at a given time, (2) a tug-of-war model in which both anterograde and retrograde motors are bound and always active but differ in their number on the cargo, and (3) a coordinate-regulation model in which both sets of motors are bound but one group is inactive [16, 17]. The observations that dynein is associated with anterograde transported cargos [22] and kinesin is associated with retrogradely transported vesicles containing synaptic components [23] argue against the substitution model of transport for SVPs. If the tug-of-war model were correct, then the shift in flux that we observe in Liprin-α mutants [Figure 4I] would correspond to a change in the number of bound active motors and a skewing of the velocity profile [24]. However, because no such shift is observed [Figure 4K], our results are most consistent with a model in which coordinate regulation mediated through Liprin-α modulates transport [16, 17]. Because Liprin-α interacts with kinesins but not dynein [Figure 4L], our data suggest that Liprin-α directly promotes kinesin activity or cargo-association [25], which then leads to dynein inhibition through some additional component(s).

In light of the observations that disruption of kinesin alters the morphology and electrophysiological properties of synapses [1, 2, 12], our observations suggest that the synaptic defects seen in mutants of LAR and the Anaphase Promoting Complex [4, 6] may be mediated in part by Liprin-α's role in axonal transport. As a scaffolding protein with multiple known partners and motors [11], Liprin-α is in an ideal position for integ-

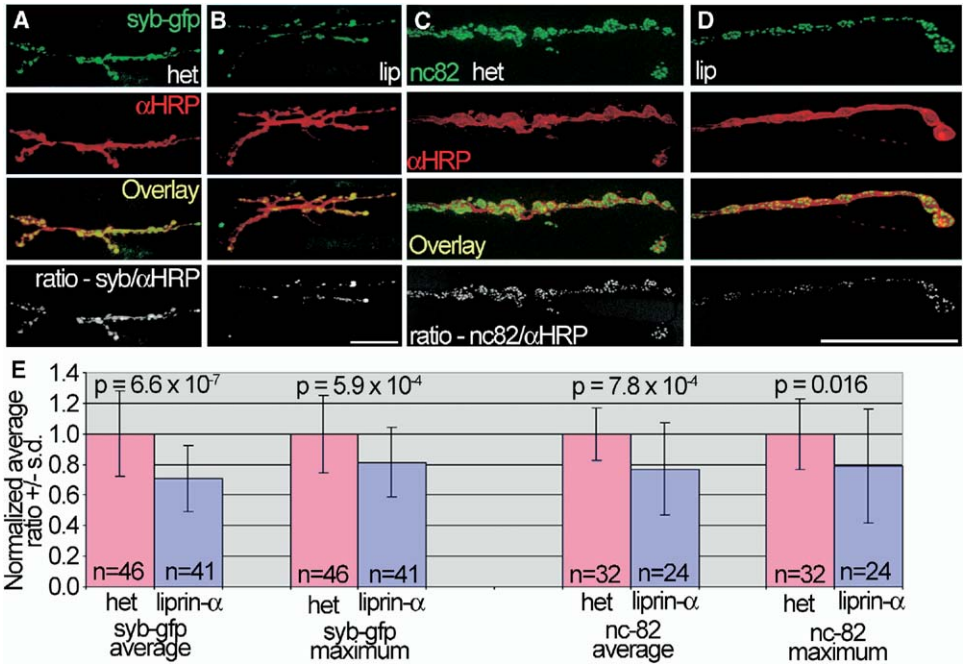

Figure 3. *Liprin-α* Is Required for Efficient Accumulation of Markers at the Synapse

(A) Distribution of nSyb-GFP compared to the internal control HRP at the NMJ in *Liprin-α* heterozygous third-instar larvae and (B) *Liprin-α* mutants. (C) Distribution of NC82 at NMJs in *Liprin-α* heterozygous third-instar larvae and (D) *Liprin-α* mutants. The intensity, but not the overall pattern of staining, is altered. The scale bar represents 10 μm. (E) The average levels and maximum intensity of staining of both markers is significantly reduced, as determined by a two-tailed t test (see Supplemental Experimental Procedures). The standard deviations are indicated for each bar.

rating and transducing information to regulate the delivery of cargoes to and from the synapse.

Supplemental Data

Supplemental Experimental Procedures and a movie are available with this article online at http://www.current-biology.com/cgi/content/full/15/7/684/DC1/.

Acknowledgments

We would like to thank Drs. T. Schwarz, K. Johnson, A. Ghose, J. Flanagan, and T. Rapoport for helpful comments, Dr. M. Ramaswami for the UAS-ung-12-gfp (i.e. UAS-nSyb-GFP), and Dr. W. Saxton for the GAL4 driver strain D42. We also thank the Bloomington *Drosophila* Stock Center at the University of Indiana for additional strains. Antibodies were kind gifts from Drs. T. Hays, L. Goldstein, H. Bellen, T. Littleton, D. Schmucker, T. Schwarz, and R. Ranjan. We thank the Developmental Studies Hybridoma Bank for antibodies. We would also like to thank Dr. J. Waters and L. Petrak at the Harvard Medical School Nikon Imaging Center for microscopy assistance. D.V.V. is a Leukemia and Lymphoma Society Scholar. Additional support was derived from a grant from the National Institute of Neurological Disorders and Stroke (N90035).

Received: October 6, 2004
Revised: February 16, 2005
Accepted: February 17, 2005
Published: April 12, 2005

References

1. Gho, M., McDonald, K., Ganetzky, B., and Saxton, W.M. (1992). Effects of kinesin mutations on neuronal functions. Science *258*, 313–316.
2. Hurd, D.D., and Saxton, W.M. (1996). Kinesin mutations cause motor neuron disease phenotypes by disrupting fast axonal transport in Drosophila. Genetics *144*, 1075–1085.
3. Schnapp, B.J. (2003). Trafficking of signaling modules by kinesin motors. J. Cell Sci. *116*, 2125–2135.
4. Kaufmann, N., DeProto, J., Ranjan, R., Wan, H., and Van Vactor, D. (2002). *Drosophila* liprin-alpha and the receptor phosphatase Dlar control synapse morphogenesis. Neuron *34*, 27–38.
5. Shin, H., Wyszynski, M., Huh, K.H., Valtschanoff, J.G., Lee, J.R., Ko, J., Streuli, M., Weinberg, R.J., Sheng, M., and Kim, E. (2003). Association of the kinesin motor KIF1A with the multimodular protein liprin-alpha. J. Biol. Chem. *278*, 11393–11401.
6. van Roessel, P., Elliott, D.A., Robinson, I.M., Prokop, A., and Brand, A.H. (2004). Independent regulation of synaptic size and activity by the anaphase-promoting complex. Cell *119*, 707–718.
7. Ahmari, S.E., Buchanan, J., and Smith, S.J. (2000). Assembly of presynaptic active zones from cytoplasmic transport packets. Nat. Neurosci. *3*, 445–451.
8. Pulido, R., Serra-Pages, C., Tang, M., and Streuli, M. (1995). The LAR/PTP delta/PTP sigma subfamily of transmembrane protein-tyrosine-phosphatases: Multiple human LAR, PTP delta, and PTP sigma isoforms are expressed in a tissue-specific manner and associate with the LAR-interacting protein LIP.1. Proc. Natl. Acad. Sci. USA *92*, 11686–11690.
9. Zhen, M., and Jin, Y. (1999). The liprin protein SYD-2 regulates the differentiation of presynaptic termini in C. elegans. Nature *401*, 371–375.
10. Wyszynski, M., Kim, E., Dunah, A.W., Passafaro, M., Valtschanoff, J.G., Serra-Pages, C., Streuli, M., Weinberg, R.J., and Sheng, M. (2002). Interaction between GRIP and liprin-alpha/SYD2 is required for AMPA receptor targeting. Neuron *34*, 39–52.
11. Zhen, M., and Jin, Y. (2004). Presynaptic terminal differentiation: Transport and assembly. Curr. Opin. Neurobiol. *14*, 280–287.

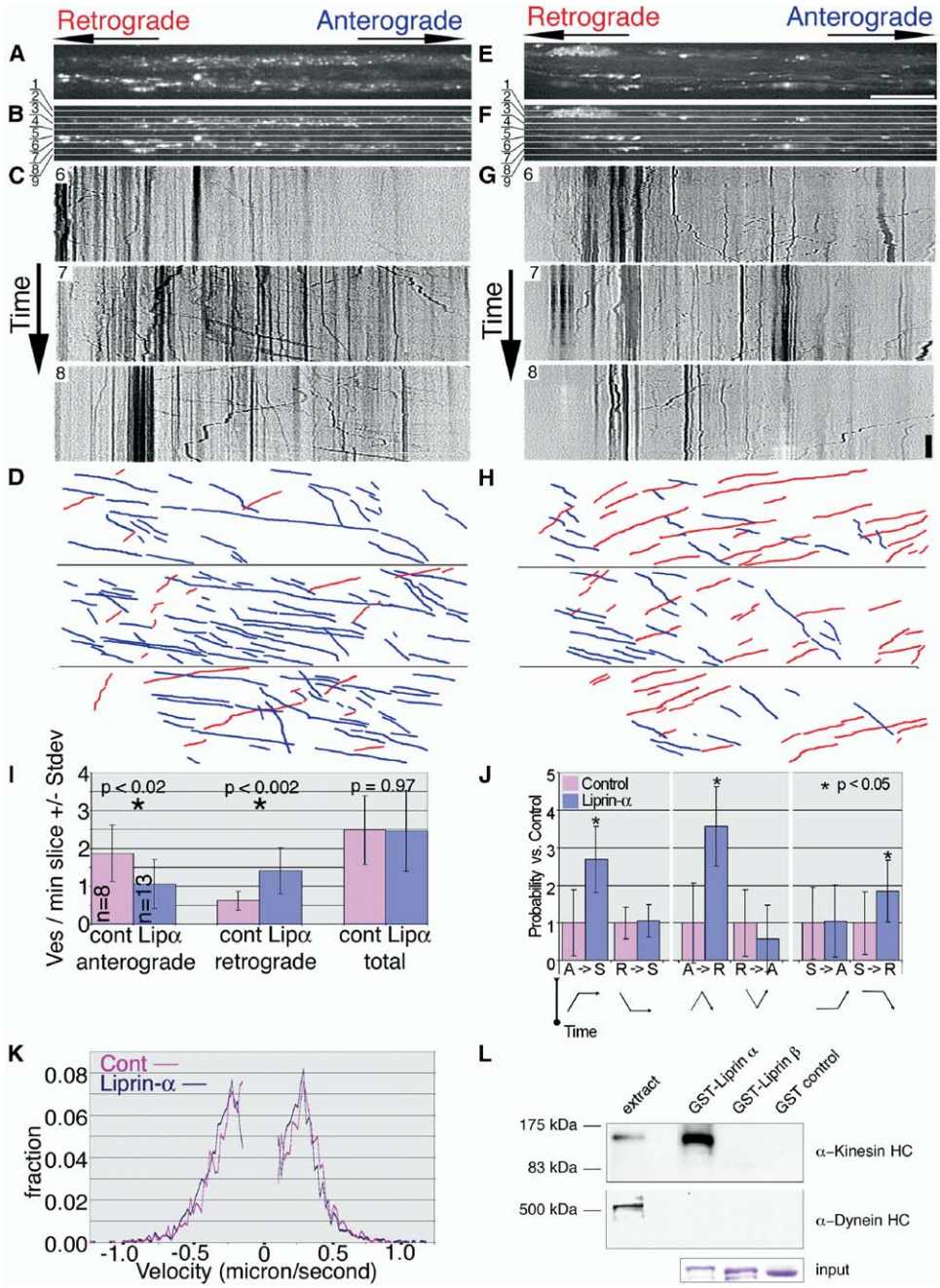

Figure 4. Loss of *Liprin-α* Decreases Anterograde and Increases Retrograde Transport

(A) A frame from a time-lapse movie of nSyb-GFP-labeled vesicle transport in *Liprin-α* heterozygous larvae.

(B) For generation of kymographs, the segmental nerve was divided into substacks numbered 1–9 as shown.

(C) Kymographs of SVP transport from the individual substacks. Vesicles moving in the anterograde and retrograde directions appear as lines with sharp slopes, and stationary vesicles appear as vertical lines.

(D) Lines drawn by hand illustrate the types of movements analyzed. Anterograde transport is shown in blue, and retrograde transport is shown in red.

(E) A frame from a time-lapse movie of nSyb-GFP-labeled vesicles in a *Liprin-α* background. A nSyb-GFP accumulation is present in the top left of the image. The scale bar represents 10 μm.

(F) The stack was divided into substacks for kymograph generation.

(G) Kymographs of SVP transport from substacks 6–8; the scale bar repesents 1 min.

(H) Lines drawn by hand illustrate anterograde and retrograde transport.

(I) Quantitative analysis of the flux of SVP; the standard deviations are indicated for each bar.

(J) The number of transitions from transport to pauses, sudden reversals, and the initiation of transport for nSyb-GFP vesicles were determined by analysis of the kymographs for *Liprin-α* heterozygous and null animals (A = anterograde, R = retrograde, and S = stop). The average probability, as compared to the control, of the event occurring ± standard deviation is shown. P values for significance levels are shown in the graph.

(K) Disruption of Liprin-α does not alter the velocity profiles of transport.

(L) GST fusion constructs of *Drosophila* Liprin-α, Liprin-β, or the GST moiety alone were used in pull-down assays from embryo extracts. Kinesin was detected with an affinity-purified rabbit α-*Drosophila* Kinesin-1 heavy chain antibody, and dynein was detected with a mouse α-dynein heavy chain antibody.

12. Hurd, D.D., Stern, M., and Saxton, W.M. (1996). Mutation of the axonal transport motor kinesin enhances paralytic and suppresses Shaker in Drosophila. Genetics *142*, 195–204.
13. Okada, Y., Yamazaki, H., Sekine-Aizawa, Y., and Hirokawa, N. (1995). The neuron-specific kinesin superfamily protein KIF1A is a unique monomeric motor for anterograde axonal transport of synaptic vesicle precursors. Cell *81*, 769–780.
14. Estes, P.S., Ho, G.L., Narayanan, R., and Ramaswami, M. (2000). Synaptic localization and restricted diffusion of a Drosophila neuronal synaptobrevin–green fluorescent protein chimera in vivo. J. Neurogenet. *13*, 233–255.
15. Laissue, P.P., Reiter, C., Hiesinger, P.R., Halter, S., Fischbach, K.F., and Stocker, R.F. (1999). Three-dimensional reconstruction of the antennal lobe in Drosophila melanogaster. J. Comp. Neurol. *405*, 543–552.
16. Welte, M.A. (2004). Bidirectional transport along microtubules. Curr. Biol. *14*, R525–R537.
17. Gross, S.P. (2004). Hither and yon: A review of bi-directional microtubule-based transport. Phys. Biol. *1*, R1–R11.
18. Zahn, T.R., Angleson, J.K., MacMorris, M.A., Domke, E., Hutton, J.F., Schwartz, C., and Hutton, J.C. (2004). Dense core vesicle dynamics in Caenorhabditis elegans neurons and the role of kinesin UNC-104. Traffic *5*, 544–559.
19. Nakata, T., Terada, S., and Hirokawa, N. (1998). Visualization of the dynamics of synaptic vesicle and plasma membrane proteins in living axons. J. Cell Biol. *140*, 659–674.
20. Huang, J.D., Brady, S.T., Richards, B.W., Stenolen, D., Resau, J.H., Copeland, N.G., and Jenkins, N.A. (1999). Direct interaction of microtubule- and actin-based transport motors. Nature *397*, 267–270.
21. Serra-Pages, C., Kedersha, N.L., Fazikas, L., Medley, Q., Debant, A., and Streuli, M. (1995). The LAR transmembrane protein tyrosine phosphatase and a coiled-coil LAR-interacting protein co-localize at focal adhesions. EMBO J. *14*, 2827–2838.
22. Hirokawa, N., Sato-Yoshitake, R., Yoshida, T., and Kawashima, T. (1990). Brain dynein (MAP1C) localizes on both anterogradely and retrogradely transported membranous organelles in vivo. J. Cell Biol. *111*, 1027–1037.
23. Koushika, S.P., Schaefer, A.M., Vincent, R., Willis, J.H., Bowerman, B., and Nonet, M.L. (2004). Mutations in Caenorhabditis elegans cytoplasmic dynein components reveal specificity of neuronal retrograde cargo. J. Neurosci. *24*, 3907–3916.
24. Hill, D.B., Plaza, M.J., Bonin, K., and Holzwarth, G. (2004). Fast vesicle transport in PC12 neurites: velocities and forces. Eur. Biophys. J. *33*, 623–632.
25. Lee, J.R., Shin, H., Choi, J., Ko, J., Kim, S., Lee, H.W., Kim, K., Rho, S.H., Lee, J.H., Song, H.E., et al. (2004). An intramolecular interaction between the FHA domain and a coiled coil negatively regulates the kinesin motor KIF1A. EMBO J. *23*, 1506–1515.

Direct Observation Demonstrates that Liprin-α Is Required for Trafficking of Synaptic Vesicles

Kyle E. Miller, Jamin DeProto, Nancy Kaufmann, Bharatkumar N. Patel, April Duckworth, and David Van Vactor

Supplemental Experimental Procedures

Volume Reconstruction of Axonal Syt Accumulations

Wild-type (*w1118*) and mutant (*Liprin*-$\alpha^{EPexR117}$/*Liprin*-α^{R60}) crawling third-instar larvae were fixed and prepared for confocal microscopy as previously described [S1]. Anti-Dsyt2 (gift of Hugo Bellen) was used at 1:1000, goat α-rabbit Alexa 488 was used at 1:400, and goat α-HRP Texas Red was used at 1:50. Larvae were imaged on a Bio-Rad Radiance 2000 (Bio-Rad Laboratories) confocal microscope configured on a Nikon E800 (Nikon Instruments, Japan). For the volume measurements of the axons and of synaptotagmin-positive areas, 3D confocal reconstructions were performed for quantitative analysis. Two 8-bit channels were analyzed for axonal volume by scanning the axon image channel (red) for intensity between 36–236 (biases against noise), size no smaller than 50 um^3; in addition, our selection fills small holes and reduces inherent noise. Within this axon volume selection, synaptotagmin-positive volume was measured in the green channel on the basis of intensity between 19.67–252, size no smaller than 0.4 um^3, with a noise-reduction tool applied. In all cases, selected areas were displayed prior to measurement to ensure that anomalous selections (such as boutons or nonaxonal tissue) were not included in the final analysis. The axons were reassembled and analyzed with Volocity 2.0 (Improvision, UK).

Frequency of nSyb-GFP Accumulations

Crawling third-instar larvae that were wild-type (*w; D42-Gal4, UAS-nSyb-GFP/TM3Sb*) or *Liprin*-α mutants (*Liprin*-α^{F3ex15}/*Liprin*-α^{IJO}; *D42-Gal4, UAS-nSyb-GFP*/+) were anesthetized in Halocarbon oil 700 (Sigma) mixed with 15%–25% chloroform titrated to a level that blocked significant contractions, mounted between a slide and coverslip, and then set aside for 5–10 min to allow the chloroform to take effect. Observations were made at ~25°C for no more than 15 min with a spinning-disk confocal fluorescence microscope controlled by MetaMorph software (Universal Imaging) with a 60×/1.4 NA Plan Apochromat objective (Nikon) and a cooled CCD camera (model ER; Hamamatsu). Confocal stacks were acquired, opened in ImageJ (National Institutes of Health), and z-projected with the maximum intensity function. The number of nSyb-GFP accumulations over the first 150 μm of the central two branches of the segmental nerves as they exit the ventral nerve cord were counted and divided by nerve length.

Electron Microscopy

Liprin-α (*Liprin*-α^{R60}/*Liprin*-α^{F3ex15}) mutants and wild-type (*w1118*) crawling third-instar larvae raised at 25°C and 60% relative humidity were prepared in parallel for EM. Larvae were dissected, fixed, and embedded as previously described [S2]. Peripheral nerve bundles in the ventrolateral domain of the abdominal segments were selected for serial section, including ISNb and SNa. Serial 100 nm sections were collected from wild-type (n = 3) and mutant (n = 3) larvae. Quantification of axonal vesicle distributions was performed in two ways: (1) The total number of vesicles in a 500 nm^2 area of axonal area was counted in a given axon from serial sections of mutant and control peripheral nerves with a mask representing 500 × 500 nm aperture placed over each negative (this data was then plotted as a function of distance along the axon in Figures 2D and 2E), and (2) accumulations of four or more vesicles in direct apposition anywhere in a given axon were counted in the same series of micrographs (this data is summarized in a bar graph showing the number of such accumulations per μm of axon length). The total axon length portrayed represents several different axon lengths, shown in series, in each genotype. Microtubules were identified on the basis of diameter, morphology, and persistence from adjacent sections.

Intensity Analysis at the NMJ

Control larvae with *Liprin*-α heterozygous over the Black cell balancer (*Liprin*-α^{IJO} or *Liprin*-α^{R60}/*In(2LR)Gla, wg^{Gla-1}, Bc^1; D42-Gal4, UAS-nSyb-GFP*/+) and mutant larvae (*Liprin*-α^{IJO}/*Liprin*-α^{R60}; *D42-Gal4, UAS-nSyb-GFP*/+) were fixed and stained with rabbit α-GFP at 1:1000 (Abcam) or mouse α-NC82 at 1:100, Texas Red α-HRP at 1:50, and then goat α-rabbit or goat α-mouse Alexa 488 at 1:400. Control and mutant larvae were prepared and imaged in parallel with illumination set at a level that prevented pixel saturation. Confocal stacks were acquired at 60× magnification on a spinning-disk confocal microscope (as described above) with 0.5 μm steps through a 10-μm-thick region that contained the NMJ. The red (HRP) and green (NC82 or nSyb-GFP) channels were obtained simultaneously. Three-dimensional confocal reconstructions were z-projected with the maximum intensity function in ImageJ. Then, the ratio of the two z-projections was calculated by dividing them with the HRP as the denominator. For each NMJ, five (12.4 um^2) regions were analyzed in the ratio image with the measure function in ImageJ. The mean of the five regions was then calculated for the average and maximum levels of intensity from the ratio image. From these values, the significance levels were calculated with a two-tailed t test. For the graph in Figure 3, these values were normalized on the control levels of staining.

Time-Lapse Imaging

Crawling third-instar larvae were anesthetized in Halocarbon oil 700 mixed with 15%–25% chloroform and imaged on a spinning-disk confocal microscope as described above. Controls included *Liprin*-α^{IJO} or *Liprin*-α^{R60}/*CyO$_{actin5C\text{-}GFP}$; D42-GAL4, UAS-nSyb-GFP* and *Liprin*-α^{F3ex15} or *Liprin*-α^{R117}/*CyO$_{actin5C\text{-}GFP}$; D42-GAL4, UAS-nSyb-GFP*, whereas the homozygous mutant combinations were *Liprin*-α^{R117}/*Liprin*-α^{F3ex15}; *D42-GAL4, UAS-nSyb-GFP* and *Liprin*-α^{IJO}/*Liprin*-α^{R60}; *D42-GAL4, UAS-nSyb-GFP*. Observations were made every 2 s on a single plane at ~25°C for no more than 15 min on a spinning-disk confocal microscope at 100×/1.4 NA. Movies were opened in ImageJ, rotated with the TransformJ plugin (TJ Rotate with a Cubic B-spline interpolation scheme), and aligned with the TurboReg plugin with the Rigid Body: Accurate setting. The stacks of images were resliced and divided into substacks, and the substacks were z-projected with the sum option to make kymographs. Lines tracing the path of the SVPs in kymographs were drawn by hand, and the slopes of the traces were determined with the "analyze particle" function of National Institutes of Health image and then exported to Excel and converted to velocities.

Analysis of Flux

To quantify transport (Figure 4I), we counted the number of nSyb-GFP-labeled objects that crossed a single point across the nerve and then divided that number by the "time of observation" to yield the flux in terms of vesicles/s. The time of observation for each axon was equal to the number of kymograph slices in which transport was evident × the number of seconds of observation.

Analysis of Transitions

Stops, starts, and reversals (Figure 4J) were operationally defined as transitions from stops or movements that lasted for a minimum of 10 s (i.e., five frames). A stop was counted when the velocity of movement was less than 0.1 μm/s.

For the analysis of stops and reversals (Anterograde to Stop,

Retrograde to Stop, Anterograde to Retrograde, and Retrograde to Anterograde), the number of each type of event was counted blind for each axon and then divided by the magnitude of flux for that axon in the appropriate direction. Two-tailed t tests were done on these values, which were then divided by the controls to convert to relative probabilities.

For starts (Stopped to Anterograde and Stopped to Retrograde), the number of events for each axon was divided by the time of observation (described above) for each axon. From these values, the average and significance levels were calculated with a two-tailed t test for each group in the control and experimental conditions. The relative probabilities were generated by dividing by the number of events in the control condition.

Analysis of Velocity Profile

Lines such as those shown in Figure 4D were drawn in separate layers in Photoshop for the analysis of the velocity profiles. These layers were saved, opened in ImageJ, made binary, and thresholded, and the "analyze particle" function was used to determine the slope and length of each line. These data were pooled and binned by velocity to generate the velocity profiles shown in Figure 4K. In total, 40,344, 26,314, 47,264, and 44,896 s of vesicle movement were analyzed, respectively, for the control in the anterograde and retrograde directions and for Liprin-α in the anterograde and retrograde directions. For each of the four groups, the velocity profiles were independently divided by the seconds of vesicle movement to normalize the data. Velocities less than 0.1 μm/s were excluded from the analysis.

GST-Fusion Protein Pull-Downs

GST-fusion protein constructs of full-length *Drosophila* Liprin-α and -β were generated by PCR with the Expand High Fidelity PCR System (Roche) and amplified with EST clones LD 27334 and RE03082, respectively (ResGen). PCR products were directionally cloned into the vector pGEX-4T-1 (Amersham Biosciences) with EcoRI and NotI. Constructs were transfected into BL21 *E. coli*, and protein expression was induced with 0.2 mM Isopropyl bD-thiogalactopyranoside (IPTG). Cells were sonicated, and supernatants were subjected to SDS-PAGE and Coomassie staining. Clones expressing the appropriately sized fusion protein were verified by sequencing and by Western-blot analysis with affinity-purified rabbit anti-*Drosophila* Liprin-α or Liprin-β antibodies. Fusion proteins were purified with Glutathione Sepharose beads (Amersham Biosciences) and dialyzed against PBS. Protein extracts from 0–20 hr AEL (after egg lay) embryos were prepared by homogenizing embryos in ice-cold PBS containing 0.2% Triton X-100, 0.2% Igepal CA-630, and protease inhibitors (Complete tablets—EDTA; Roche) in a dounce homogenizer. The homogenate was centrifuged at 10,000 g for 1 hr at 4°C, and the supernatant was collected. For the GST-fusion protein pull-downs, 2 μg of GST-Liprin-α and GST-Liprin-β and 4 μg of GST (control) were incubated with 1 ml of embryo extract (2 mg/ml protein) for 4 hr at 4°C. Twenty-five microliters of PBS-washed Glutathione Sepharose beads was added and incubated for an additional 1 hr. The samples were centrifuged, and the beads were washed three times with 1 ml ice-cold PBS containing 0.2% Igepal CA-630. An equal volume of 2$\times$ Laemmli reducing sample buffer was added to the beads and heated at 98°C for 10 min and centrifuged. Samples were subjected to SDS-PAGE, transferred onto nitrocellulose, and immunoblotted with an anti-*Drosophila* Kinesin I heavy-chain antibody (1:1000 AKIN01; Cytoskeleton) or the mouse anti-fly dynein heavy-chain antibody P1H4 (1:2000, Tom Hays [S3]) and a goat anti-rabbit HRP-conjugated secondary antibody (Jackson ImmunoResearch). Enhanced chemiluminescence (ECL) was performed to visualize the bands (Amersham Biosciences).

Supplemental References

S1. Kaufmann, N., DeProto, J., Ranjan, R., Wan, H., and Van Vactor, D. (2002). Drosophila liprin-alpha and the receptor phosphatase Dlar control synapse morphogenesis. Neuron *34*, 27–38.

S2. Schuster, C.M., Davis, G.W., Fetter, R.D., and Goodman, C.S. (1996). Genetic dissection of structural and functional components of synaptic plasticity. I. Fasciclin II controls synaptic stabilization and growth. Neuron *17*, 641–654.

S3. McGrail, M., and Hays, T.S. (1997). The microtubule motor cytoplasmic dynein is required for spindle orientation during germline cell divisions and oocyte differentiation in Drosophila. Development *124*, 2409–2419.